Deformation Mechanism of Elastomeric Block Copolymers Having Spherical Domains of Hard Segments under Uniaxial Tensile Stress[1]

Takashi Inoue, Masahiko Moritani, Takeji Hashimoto, and Hiromichi Kawai*

Department of Polymer Chemistry, Faculty of Engineering, Kyoto University, Kyoto, Japan. *Received January 19, 1971*

ABSTRACT: Elastomeric block copolymers are two-phase systems composed of spherical domains of a plastic component of colloidal dimensions dispersed in a matrix of rubber component. The deformation mechanism of such copolymers was investigated for A–B-type and A–B–A-type block copolymers of styrene and isoprene, as well as for mixtures of the A–B-type block copolymer with each corresponding homopolymer, by means of simultaneous measurements of the tensile stress–strain relation, small-angle light scattering, and small-angle X-ray scattering. The deformation of these materials, except for that of a mixture of the A–B-type block copolymer with homopolyisoprene, is accompanied by formation of heterogeneity in density over a considerable region which is much larger in size than the microheterogeneous structures of the materials, *i.e.*, the domain structures formed by the microphase separation of the block segments. The elastomeric properties of the block copolymers at relatively higher elongations are associated with the formation of this localized region of lower density rather than with the uniform deformation of the rubber matrix between the hard spherical domains. On the other hand, for the exceptional specimen, the mixture of the A–B-type block copolymer with homopolyisoprene, the formation of such a localized heterogeneous region is prevented by the flow of homopolyisoprene molecules, which are not anchored to the surface of the spherical domains of polystyrene, into the region.

In recent years a class of linear amorphous block copolymers, such as the styrene–butadiene block copolymers and the polyester–MDI block copolymers, has attracted attention. These are named "thermoplastics" or "segmented elastomers" because they have characteristic mechanical properties similar to those of the conventional reinforced rubber vulcanizates at service temperature, but without cross-linking and filler-modifying processes.[2] The elastomeric properties of these materials have been investigated by means of tensile stress–strain relations. Speculations have been made about their molecular structures without taking account of deformation mechanisms of microheterogeneous structures which result from microphase separation of the block segments, owing to the molecular architecture and the preparation conditions of the bulk materials.[3]

In order to understand the elastomeric properties in further detail, some rheooptical studies using birefringence[4–6] and infrared dichroism[7] have been carried out. However, it should be noted that such optical quantities are related to the optical anisotropies of chemical bonds and represent average values of the orientation of the segments of the chain molecules. Measurements associated with the chain segments are too small to provide definite information on the deformation mechanism of the microheterogeneous structures, *i.e.*, the domain structures of these materials. In contrast, light scattering is a phenomenon which is very sensitive to the fluctuations of optical anisotropy and density of a system having correlation distances of colloidal dimensions. Fluctuations having shorter correlation distances than the above, *i.e.*, several hundred ångströms, may be investigated by small-angle X-ray scattering. These scattering techniques are powerful tools for investigating the deformation mechanism of a two-phase polymer system and especially for examining changes in the domain structures.

In this paper some results of rheooptical studies using small-angle light scattering and X-ray scattering techniques will be discussed for uniaxial stretching of film specimens of styrene–isoprene block copolymers and of mixtures of the copolymers with the corresponding homopolymers. All the specimens have spherical domains of polystyrene component dispersed in a matrix of polyisoprene component. Some fundamental deformation mechanisms for the elastomeric behavior of these materials, relating to their domain structure and molecular architecture, will be explained.

Procedures and Results

Test Specimens. An A–B-type block copolymer of styrene–isoprene ($\bar{M}_n$ 27.8 × 10^4, 18.5 wt % styrene) designated SI, an A–B–A-type block copolymer of styrene–isoprene–styrene ($\bar{M}_n$ 59.5 × 10^4, 23.0 wt % styrene) designated SIS, homopolystyrene ($\bar{M}_n$ 3.34 × 10^4) designated PS, and homopolyisoprene ($\bar{M}_n$ 39.8 × 10^4) designated PI, were synthesized by a living polymerization technique initiated by *n*-butyllithium for both the A–B-type block copolymer and the homopolymers[8] and by tetramethylenedilithium for the A–B–A-type block copolymer,[9] all in tetrahydrofuran (THF) at −78°. Film specimens were prepared by casting the mono- or bicomponents from 5% toluene solutions of these polymers. The domain structures of the cast films were examined with an electron microscope with use of the OsO_4 fixation technique.[10]

Figure 1 shows the electron micrographs of ultrathin sections of about 350-Å thickness cut normal to the film sur-

(1) Presented in part before the Symposium on Colloidal and Morphological Behavior of Block and Graft Copolymers, Division of Polymer Chemistry, 160th National Meeting of the American Chemical Society, Chicago, Ill., Sept 14, 1970, and in part before the 18th Annual Symposium on Rheology, Odawara, Japan, Oct 8, 1970.

(2) (a) M. Morton, J. E. McGrath, and P. C. Juliano, *J. Polym. Sci., Part C*, **No. 26**, 99 (1969); (b) S. L. Cooper and A. V. Tobolsky, *Polym. Prepr., Amer. Chem. Soc., Div. Polym. Chem.*, **8**, 52 (1967).

(3) R. Zelinski and C. W. Childers, *Rubber Chem. Technol.*, **41**, 161 (1968).

(4) E. Fischer, and J. F. Henderson, *J. Polym. Sci., Part C*, **No. 26**, 149 (1969).

(5) R. S. Stein and G. L. Wilkes, *ibid., Part A-2*, **7**, 1525 (1969).

(6) D. G. LeGrand, *ibid., Part B*, **7**, 579 (1969).

(7) R. S. Stein, private communication.

(8) T. Inoue, T. Soen, T. Hashimoto, and H. Kawai, *J. Polym. Sci., Part A-2*, **7**, 1283 (1969).

(9) T. Uchida, T. Soen, T. Inoue, and H. Kawai, *ibid., Part A-2*, in press.

(10) K. Kato, *Polym. Eng. Sci.*, **7**, 38 (1967).

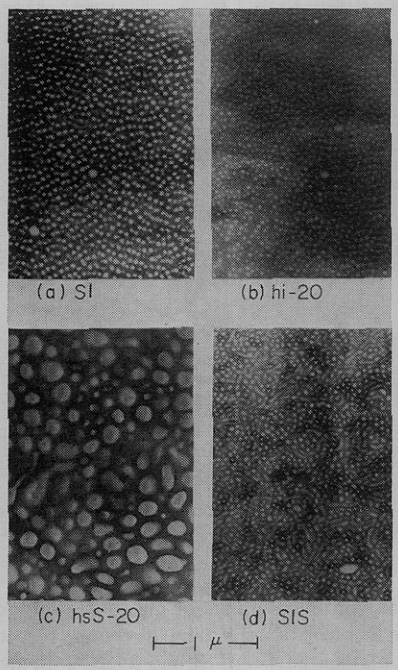

Figure 1. Electron micrographs of ultrathin sections cut normal to the surfaces of the stained (OsO_4) film specimens cast from 5% toluene solutions of styrene–isoprene block copolymers: (a) A–B-type block copolymer of styrene–isoprene, (b) mixture of the A–B-type block copolymer with homopolyisoprene, (c) mixture of the A–B-type block copolymer with homopolystyrene, (d) A–B–A-type block copolymer of styrene–isoprene–styrene.

faces. The domain structure of SI (Figure 1a) may be characterized as spheres of styrene component dispersed in a matrix of isoprene component, with the radii of the spheres measuring about 200 Å.[8] Specimen hi-20 is a binary mixture of 80 wt % SI and 20 wt % PI. As seen in Figure 1b, PI is solubilized in the matrix of the isoprene block of the copolymer SI; this increases the distance between the polystyrene spherical domains (*cf.* Figure 1a).[11] Specimen hsS-20 is a binary mixture of 80 wt % SI and 20 wt % PS. As seen in Figure 1c, PS is solubilized, by contrast, in the spherical domains of the styrene block of the copolymer SI, which enlarges the size of the spherical domains (again *cf.* Figure 1a).[11] The domain structure of SIS (Figure 1d) may be characterized as spheres of styrene component dispersed in a

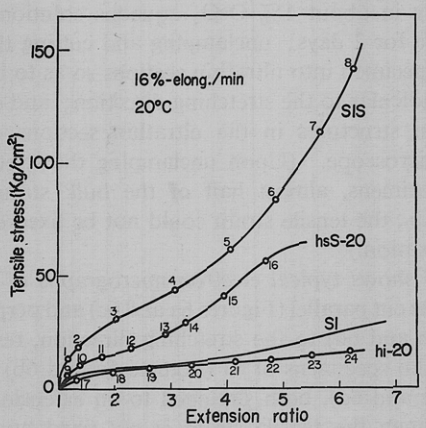

Figure 2. Tensile stress–strain relations of the film specimens under a constant rate of elongation, 16%/min, at 20°.

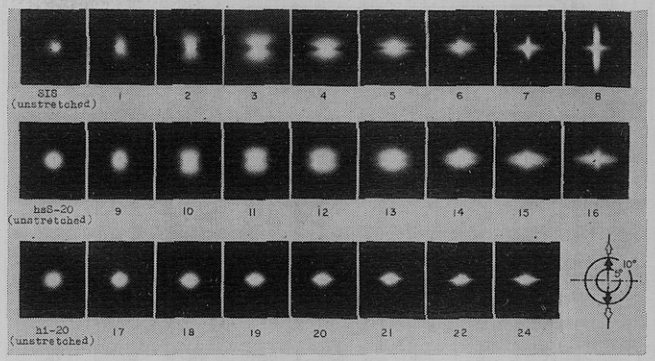

Figure 3. V_v light scattering patterns from the film specimens at various stretched states indicated by the same numbers as those along the stress–strain curves in Figure 2. The light source is a He–Ne gas laser having a wavelength of 6328 Å. The scale of scattering angles is indicated in the lower right-hand corner, together with the polarization directions of the optical system (solid arrows) and the stretching direction of the film specimens (open arrows), both with respect to the V_v patterns.

matrix of isoprene component, some of these spheres being interconnected to form short rodlike domains. In summary, every specimen has a very definite two-phase structure, a domain structure of hard plastic spheres dispersed in a soft rubber matrix, just like a filler-reinforced rubber.

Tensile Stress–Strain Behavior. The tensile stress–strain relation of 0.1-mm thick film specimens was measured under a constant rate of elongation, 16%/min, at 20°. All specimens behave, as illustrated in Figure 2 (and in Figure 11), like rubber vulcanizates. The SIS specimen is the stiffest and the most elastomeric, while the hi-20 specimen is the softest and the least elastic, showing a rather low leveling-off stress, and lacking the rapid rise in stress at higher elongations. It is noted that the SIS specimen, whose styrene content is 23 wt %, has a higher initial Young's modulus and larger tensile strength than hsS-20, whose styrene content is 36 wt % total. This is inconsistent with the filler-reinforcing effect of the styrene component, and will be explained later in terms of the difference between the molecular arrangements of the isoprene blocks in the rubber matrix.

Small-Angle V_v Light Scattering Patterns. The photographic light scattering technique[12,13] was used for the small-angle light scattering experiment. The incident beam was provided by a He-Ne gas laser apparatus, Model NAL-705Z, Nippon Kagaku Kogyo, Inc. The well-collimated beam, polarized parallel to the stretching direction by using a polarization rotator, Model 310, Spectra Physics Inc., and monochromatized at a wavelength of 6328 Å, was incident to the film surface.

The H_v (cross polarized) light scattering pattern could not be detected from any of the film specimens at any of the stretched states along the stress–strain plots in Figure 2. On the other hand, the characteristic change of the V_v (parallel polarized) scattering pattern with extension ratio was observed for all specimens, as illustrated in Figure 3. The numbers 1–24 attached to the patterns correspond to those in Figure 2 along the stress–strain plots. In Figure 3, the scattering patterns from the SI specimen were omitted because of their similarity to those from the SIS and hsS-20 specimens. It may be noted that the marked change of the pattern with extension ratio observed for the SIS and hsS-20 specimens is observed much less for the hi-20 specimen.

(11) T. Inoue, T. Soen, T. Hashimoto, and H. Kawai, *Macromolecules*, 3, 87 (1970).

(12) A. Plaza and R. S. Stein, *J. Polym. Sci.*, **40**, 267 (1959).
(13) R. S. Stein and N. B. Rhodes, *J. Appl. Phys.*, **31**, 1837 (1960).

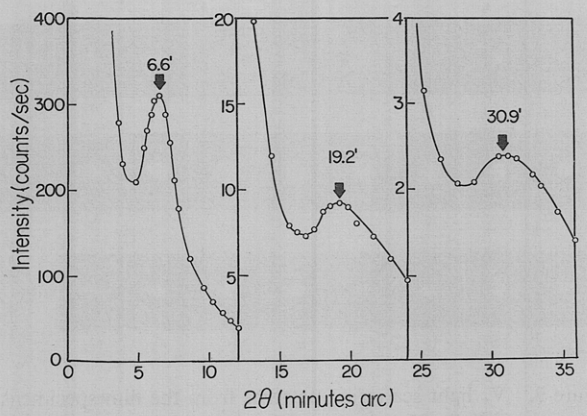

Figure 4. Intensity distribution of small-angle X-ray scattering from an unstretched film specimen of SI, showing at least three distinctive peaks.

Small-Angle X-Ray Scattering. Small-angle X-ray scattering was investigated by using a rotating-anode-type X-ray generator, Model 2C, Rigaku Denki, Inc., and an auto-scanning-type goniometer equipped with a slit collimator system. The incident beam was Ni-filtered Cu Kα radiation. Times required for 1000 counts were measured (fixed count method) as a function of scattering angle at various azimuthal angles, and the data were reduced to relative intensity distribution as counts per second after correcting for background intensity and absorption.

Figure 4 shows an intensity distribution of the X-ray scattering, at a given azimuthal angle, from an unstretched film specimen of about 0.5-mm thickness prepared by combining the SI specimen of about 0.1-mm thickness. As seen in the figure, the scattering intensity decreases remarkably with increasing scattering angle, and shows at least three distinctive peaks at $2\theta = 6.6$, 19.2, and 30.9′, up to scattering angles of 35′. Dependence of the intensity distribution on the azimuthal angle was not observed and is not shown in the figure.

On the other hand, when the specimen is stretched, the intensity distribution becomes dependent on the azimuthal angle, so that the first peak at $2\theta = 6.6'$ shifts to lower and higher scattering angles in meridional and equatorial directions, respectively, but the second and third peaks do not shift. Figure 5 shows the change of intensity distribution in the meridional direction upon stretching, up to extension ratios of 2.0, for the above SI specimen. The data demonstrate a definite shift of the first peak from $2\theta = 6.6'$ in the unstretched state to $2\theta = 4.9'$, but no shift of the second and third peaks.

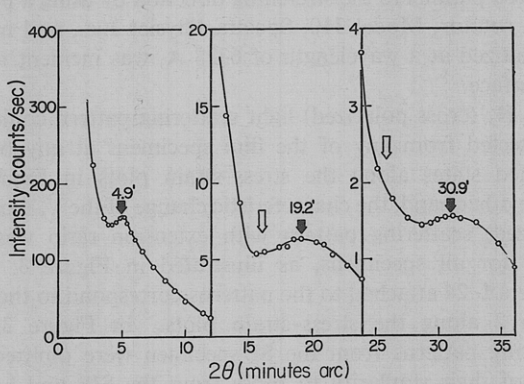

Figure 5. Intensity distribution of small-angle X-ray scattering at the meridional direction from a film specimen of SI stretched up to an extension ratio of 2.0, showing a shift of the first peak to smaller scattering angles but no shift of the second and third peaks. Open arrows show the new peak positions if the spherical hard domains are deformed by an extension ratio of 1.2.

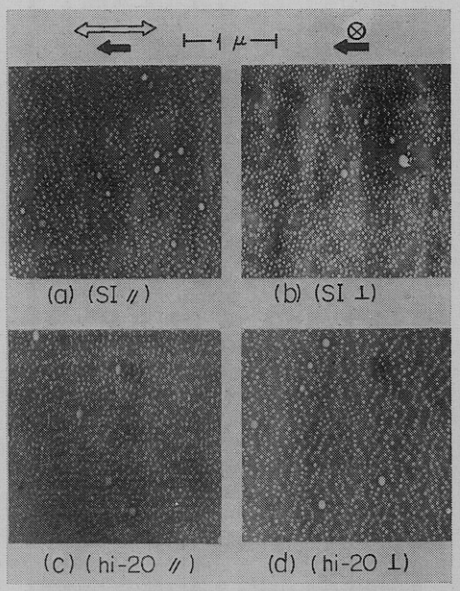

Figure 6. Electron micrographs of ultrathin sections cut parallel and perpendicular to the stretching direction, respectively, from OsO_4-stained film specimens of SI and hi-20, both stretched to an extension ratio of 4.0, where open arrows indicate the stretching direction and solid arrows show the cutting direction of the specimens. The extension ratio is not necessarily fixed enough by the OsO_4 fixation, but is rather recovered to almost half of the bulk strain.

The change of the scattering intensity distribution with stretching of the specimens was measured mainly in the meridional direction in order to investigate the deformation mechanism of the domain structure in terms of the change of interdomain distance along the stretching direction.

Electron Microscopic Observation of the Morphology of Stretched Specimens. The domain structures of the specimens in their stretched states were also examined with an electron microscope by use of the OsO_4 fixation technique. The experimental procedure consisted of stretching the film specimen uniaxially to a given extension ratio under almost the same conditions as for the stress–strain data plotted in Figure 2; clamping the stretched specimen between two metallic flanges; soaking the stretched and clamped specimen immediately in about 1% OsO_4 aqueous solution at room temperature for 2 days; unclamping and cutting the stained and fixed specimen into ultrathin sections so as to be parallel and perpendicular to the stretching direction; and examining the domain structures in the ultrathin sections under the electron microscope. (Upon unclamping the stretched and stained specimens, almost half of the bulk strain was recovered; *i.e.*, the tensile strain could not be fixed enough by the OsO_4 fixation.)

Figure 6 shows typical electron micrographs of the ultrathin sections cut parallel (Figures 6a and 6c) and perpendicular (Figures 6b and 6d) to the stretching direction, respectively, from the film specimens of SI (Figures 6a and 6b) and hi-20 (Figures 6c and 6d), both stretched to an extension ratio of 4.0. Although the tensile strain is not fixed by the OsO_4 fixation, as mentioned above, it can at least be seen (from Figures 6a and 6b) that, for stretched SI, regions where the concentration of spherical domains dispersed in the rubber matrix is much lower are found, but (Figures 6c and 6d) for the stretched hi-20, such distinctive heterogeneities as the

above rarely appear, except for row orientation and "V-shaped" patterns of domain arrangement (Figure 6d), as suggested by Beecher, *et al.*[14] In every figure, especially in Figure 6c, the dispersed domains seem to be deformed from spherical to spheroidal. This deformation correlates, however, with the cutting direction, indicated at the tops of the respective columns of the figures by the solid arrows, rather than with the stretching direction, indicated by the open arrow.

Discussion

Deformation of Spherical Domains and Change of Interdomain Distance. The intensity distribution of X-rays scattered from a two-phase system, where spherical domains of A component, uniform in size (radius R_A), are dispersed in a matrix of B component, is given by a Zernicke–Prins-type equation[15]

$$I(h) = NF^2(U)[1 + (N/V)\int[P(R) - 1]\exp(ihR)\mathrm{d}R] \quad (1)$$

where the structural factor $F^2(U)$ is given by

$$F^2(U) = [(\rho_A - \rho_B)(4/3)\pi R_A{}^3(3/U^3)(\sin U - U\cos U)]^2 \quad (2)$$

N is the number of domains dispersed within an irradiated volume V, $U = hR_A$, $P(R)$ is the pair correlation function of mutual arrangement of the domains, $(\rho_A - \rho_B)$ is the electron density difference between the A and B phases, $h = ks$, $k = 2\pi/\lambda'$, $h = |h| = (4\pi/\lambda')\sin\theta$, where λ' is the X-ray wavelength in the system, s is the scattering unit vector, and 2θ is the scattering angle. The total scattering is composed of the single-domain scattering, the first term on the right-hand side of eq 1, and the interference scattering between the domains, the second term on the right-hand side of eq 1.

It is well known that the interference scattering term in eq 1 gives rise to a maximum of scattered intensity at nonzero scattering angles if the domains are present at high concentration.[15] The position of the intensity maximum depends in a very complicated way on the domain arrangements, and only a few kinetic theories give interpretations of this maximum in terms of the domain arrangements, without giving any analytical solution.

Here, as has been proposed by several authors,[16–19] the arrangement of the spherical domains of the block copolymers may be postulated as forming a macrolattice, and the interdomain distance D may be calculated from the position of the maximum by using the Bragg relation, $\lambda' = 2D\sin\theta$. The value of D calculated from the first peak in Figure 4 for unstretched SI is 802 Å.

The structure factor, $F^2(U)$, *i.e.*, the scattering intensity distribution from an isolated spherical domain, varies as a function of h in a series of maxima and minima of ever decreasing amplitude. It has been shown mathematically by Yudowitch[20] that the peak positions of these maxima are hardly affected by the interference scattering. Thus, the radius R_A can easily be determined from these peak positions, providing that the order of maxima can be assigned properly. By assignment of the second and third peaks in Figure 4 for unstretched SI as the first- and second-order maxima, the calculated value of R_A is 250 Å, which is somewhat larger than the value obtained from the electron microscopic observation. (This may be due to the overstaining effect of OsO_4, *i.e.*, OsO_4 may deposit not only in the isoprene matrix but also in parts of the styrene domain near the interface, thereby decreasing the radius of the domain in the electron microscopic observation.)

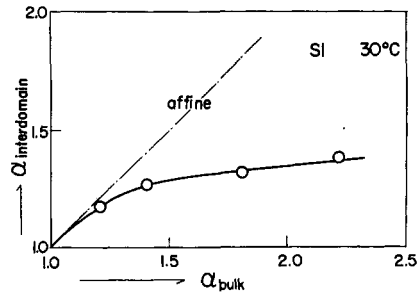

Figure 7. Plot of the extension ratio of the interdomain distance determined from small-angle X-ray scattering from a film specimen of SI, against that of the bulk specimen. The plot shows deviation from the affine deformation line passing through the origin with a slope of 45°.

The above assignment of the three peaks in Figure 4 is reasonable when compared with the electron microscopic observations, and furthermore satisfies the stoichiometric relations between R_A, D, and the volume fraction of the spherical domains. The result is the three-dimensional domain structure of the unstretched SI specimen: spherical domains of 250-Å radius hexagonally packed with interdomain distances of 802 Å.

As described in the previous section, the interference peak measured at the meridional direction shifts to smaller scattering angles with stretching. This suggests that the interdomain distance along the stretching direction is elongated. In Figure 7, the extension ratio of the interdomain distance, $\alpha_{\text{interdomain}}$, is plotted against that of the bulk specimen, α_{bulk}. As seen in the figure, the change of the interdomain distance is followed by an affine deformation only at relatively small extension ratios, and then gradually deviates from the affine deformation given by a chain line passing through the origin with a slope of 45°. This deviation further suggests that the internal strain is localized at particular points rather than distributed so uniformly within the system as to further widen the interdomain distance at higher extension ratios of α_{bulk}.

If a spherical domain undergoes uniaxial deformation at constant volume, the radius is extended by a factor γ in the stretching direction and contracted by a factor $\gamma^{-1/2}$ in the transverse directions. The structure factor of the resulting prolate spherical domain with semimajor axis γR_A and semiminor axis $\gamma^{-1/2}R_A$ is given by modifying eq 2 by replacement of U with U'[21,22]

$$U' = hR_A\gamma^{-1/2}[1 + (\gamma^3 - 1)\cos^2\theta\cos^2\mu]^{1/2} \quad (3)$$

(14) J. F. Beecher, L. Marker, R. D. Bradford, and S. L. Aggarwal, *J. Polym. Sci., Part C*, **No. 26**, 117 (1969).
(15) A. Guinier and G. Fournet, "Small-Angle Scattering of X-rays," Wiley, New York, N. Y., 1955, Chapter 2.
(16) H. Hendus, K. H. Illers, and E. Ropte, *Kolloid-Z. Z. Polym.*, **216**, 110 (1967).
(17) G. A. Harpell and C. E. Wilkers, *Polym. Prepr., Amer. Chem. Soc., Div. Polym. Chem.*, **10**, 678 (1969).
(18) D. McIntyre and E. Campos-Lopez, "Block Polymers," S. L. Aggarwal, Ed., Plenum Press, New York, N. Y., 1970, p 19.
(19) D. McIntyre and E. Campos-Lopez, *Macromolecules*, **3**, 323 (1970).
(20) K. L. Yudowitch, *J. Appl. Phys.*, **20**, 174 (1949)
(21) A. L. Patterson, *Phys. Rev.*, **56**, 972 (1939).
(22) R. J. Samuels, *J. Polym. Sci., Part C*, **No. 13**, 37 (1966).

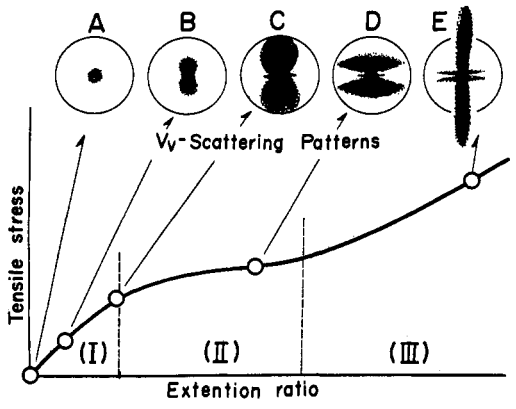

Figure 8. Schematic diagrams showing typical changes of a V_v light scattering pattern from a film specimen as a function of extension ratio.

where μ is the azimuthal angle with respect to the semimajor axis.

Equations 2 and 3 show that the second and third peaks of the scattered intensity along the meridional direction shift to smaller angles if the spherical domain deforms to the spheroidal domain. For example, the open arrows in Figure 5 indicate the positions of the second and third peaks calculated from eq 2 and 3 by assuming R_A = 250 Å and γ = 1.2. The positions of the peaks change appreciably with the deformation of the domain. When compared with the experimental results for the SI specimen in the figure, no definite deformation of the spherical domain to the spheroidal domain can be detected. That is, it may be concluded that the spherical domains of the styrene component are hardly deformed.

Deformation Mechanism Interpretation of V_v Light Scattering Patterns. The fact that H_v light scattering was not detected from any specimen in a stretched state suggests that correlated fluctuation of local anisotropy is hardly present[18] in the specimens. Therefore, the problem to be discussed must be mostly centered about the density fluctuation of the system due to the extension of the specimen.

Despite the significant difference in molecular architecture and domain structure among the film specimens, the characteristic change of the V_v light scattering pattern with extension ratio is summarized in Figure 8 in terms of a common series of schematic diagrams, with the exception of that for hi-20, for which the change is less remarkable than for the others. The deformation process may be divided, as illustrated in Figure 8, into the following three regions: region I, where the tensile stress increases rapidly with extension ratio and the C-type pattern grows *via* A- and B-type patterns; region II, where the rapid increase in stress levels off and the C-type pattern becomes flat to give the D-type pattern; and region III, where the stress increases rapidly again and a streak spreading in the stretching direction grows continuously, resulting in an E-type pattern, while the D-type pattern degenerates.

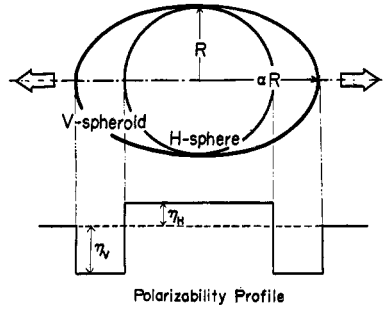

Figure 9. A proposed model, and its polarizability profile, for the formation of localized heterogeneity in lower density regions in response to external mechanical excitation.

The circularly symmetric pattern in the unstretched state of each specimen (A-type pattern in Figure 8) is ascribed to the density fluctuation due to the two-phase structure. Strictly speaking, it must arise from the long-range correlation of the spherical domains dispersed in the matrix.[23] Anisotropy in the long-range correlation, which may be generated by the stretching, would give a change of the circular A-type pattern to an elliptical one so that its major axis is perpendicular to the stretching direction, the new pattern remaining in almost the same range of scattering angles as that for the circular pattern.[15]

This is realized in the case of hi-20, the third series in Figure 3. In addition, the deformation, if any, of the spherical domains of the stryene component may not affect the scattering pattern in such a range of small scattering angles as seen in B- through E-type patterns, because the dimension of the spherical domains of the specimens ranges from about 200 to 700 Å. In other words, the characteristic change of the V_v patterns in the B through E types cannot be interpreted in terms of any changes in the heterogeneity parameters of the spherical domains themselves,[23] and one cannot help but postulate a new fluctuation in optical density within the stretched system. The problem to be discussed is the new fluctuation and its geometrical relation to the domain structures.

The two-phase structure of all the specimens is composed of spherical domains of styrene component dispersed in the rubber matrix of isoprene chains which are securely anchored in the domains and which spread out from the interfaces to compose the rubber matrix. The structural part most easily deformed by the external stress must be the rubber matrix between the spherical domains. As suggested from the investigation of small-angle X-ray scattering, the interdomain distance increases with stretching. The deformation may be accompanied by a decrease in the segment density of the matrix between the domains along the stretching direction, since the domains are relatively closely packed, thus anchoring the isoprene chains and preventing them from flowing freely into the lower density region. The lower density regions in the matrix may not be distributed uniformly everywhere between the domains when the extension ratio of the specimen becomes relatively large. An inhomogeneous deformation composed of the lower density region (V region) and the relatively undisturbed region (H region) may be assumed to represent a new model for the structural element resulting in the V_v scattering patterns in response to the external stress. In summary, then, irrespective of the size of the domain structures of the specimens, a spherical H region of radius R surrounded by a spheroidal V region of major axis αR, as illustrated in the upper half of Figure 9, may be assumed to represent the inhomogeneous deformation.

A polarizability profile of the model is also illustrated in the lower half of Figure 9, where η_H and η_V are the mean fluctuations in the polarizability of the H and V regions, respectively. The intensity of scattered light from the model is given by

(23) M. Moritani, T. Inoue, M. Motegi, and H. Kawai, *Macromolecules*, 3, 433 (1970).

$$I = (3CV)^2[(\eta_H + \eta_V)(\sin U - U\cos U)/U^3 - \alpha\eta_V(\sin U' - U'\cos U')/U'^3]^2 \quad (4)$$

where $U = hR$, $U' = U[1 + (\alpha^2 - 1)\cos^2(\theta/2)\cos^2\mu]^{1/2}$, $h = (4\pi/\lambda'')\sin(\theta/2)$, θ is the scattering angle, μ is the azimuthal angle, λ'' is the wavelength of the scattered light within the system, C is a proportionality constant, and V is the volume of the spherical H region.

Equation 4 gives various types of scattering patterns when the values of R/λ'', α, and (η_V/η_H) are varied. A series of V_v patterns with $R/\lambda'' = 6.0$ gives the closest agreement with the experimental results in Figure 3. Some of the results, obtained by varying the values of α from 1.0 through 4.0 and of (η_V/η_H) from 0.1 through 1.5, are shown in Figure 10 to follow the change of the pattern in Figure 8.

The formation process of the C-type pattern in Figure 8 may be realized by going from (a) to (b) to (c) in Figure 10, and the flattening process of the C-type pattern into the D-type pattern in Figure 8 may be realized by the change from (d) to (e) to (f) in Figure 10. Hence, according to this model, the deformation process in region I in Figure 8 may correspond to the formation of the V region in the specimen, while the deformation process in region II may correspond to a process where the density of the V region decreases still further, with the size of the region remaining almost constant (increase of η_V/η_H with constant R and α).

On the other hand, the E-type pattern, which has a strong streak spreading in the stretching direction, may correspond to a growth of a sort of microvoid as an ultimate stage of the V region. The degeneration of the D-type pattern and, in contrast, the generation of the streak in region III suggest a process wherein transformation of some of the V regions into microvoids is accompanied by relaxation of the stress concentration in the V region. Judging from the fact that the streak spreads in the stretching direction, the void must propagate in the direction perpendicular to the stretching direction.[15]

The fact that the change in the interdomain distance with stretching deviates from the affine deformation line, as illustrated in Figure 7, may suggest that the majority of the deformation energy is utilized in forming the V region and only a fraction of the energy is used for the elongation of the interdomain distance in the H region. The relatively sharp interference peak in the X-ray scattering from the stretched specimen, as shown in Figure 5, may also suggest that, even in the highly stretched states, the regularity in the domain arrangement in the H region is not disturbed to any extent.

Suggestions from Electron Microscopy. The concept of the formation of the V and H regions in these two-phase materials at stretched states is directly supported by the electron micrographs, as demonstrated in Figure 6. For example, for the stretched SI specimen in Figures 6a and 6b, the regions where the domain concentration is much lowered can be confidently designated as V regions. However, the size of the region is apparently smaller than the value of R obtained from the light scattering analysis, probably because of the considerable recovery of bulk strain of the stained specimen, as mentioned before.

In addition, Beecher, *et al.*, have investigated the change in the morphology with stretching of a thin film of Kraton 101 with the electron microscope by use of the OsO_4 fixation technique.[14] They have suggested that deformation of the spherical domains of polystyrene, which in our study cannot be detected from the X-ray scattering for the SI specimen,

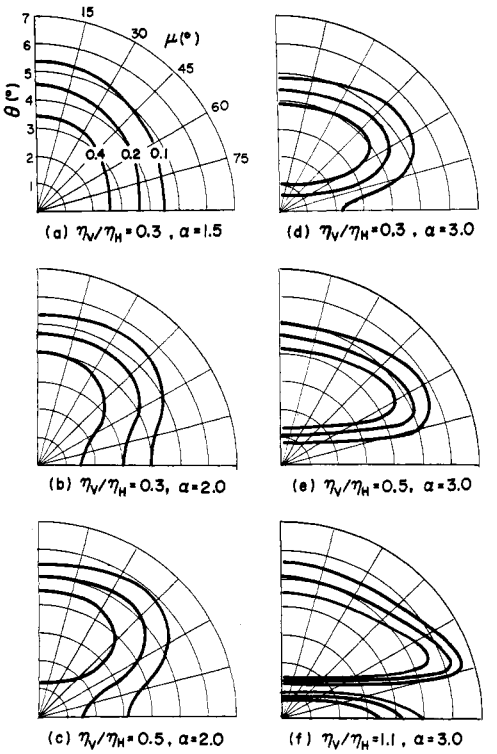

Figure 10. Contour plot of the V_v light scattering pattern obtained from eq 4 by assuming $R/\lambda'' = 6.0$ and varying (η_V/η_H) from 0.3 to 1.1 and α from 1.5 to 3.0.

occurs concurrently for different groups of the spherical domains in an area of about 1 μ^2 and must correspond to the V region.

For the stretched hi-20 specimen, on the other hand, the region corresponding to the V region is almost absent, as illustrated in Figures 6c and 6d. This is consistent with the results of the light scattering, which do not show any marked change of the V_v pattern such as are observed for the other specimens. That is to say, the deformation of the hi-20 specimen may be quite homogeneous and is not accompanied by any definite formation of V regions.

Suggestions from Molecular Architecture. The concept of heterogeneous deformation may also be supported by consideration of the differences in molecular architecture among the specimens.

The difference between the light scattering behavior of the hi-20 specimen and that of the other specimens may be explained in terms of the differences in molecular architecture in the matrix phase between the specimens. The matrix phase of hi-20, a binary mixture of SI and PI, is composed of polyisoprene block chains of SI and the solubilized homopolymer chains of PI. On the other hand, the matrices of the other specimens, SI, SIS, and hsS-20, are composed of only the isoprene blocks of the respective copolymers.

In the case of the hi-20 specimen, the solubilized PI chains extend the distance between the spherical domains of the styrene component and are not anchored to the domains; thus the PI chains may easily flow into the lower density regions to average out the density uniformly. In contrast to the other specimens, where the isoprene blocks are anchored to the spherical domains, this prevents the formation of the V region and the marked changes of the V_v pattern with stretching.

In the case of the SIS specimen, there must be, in addition,

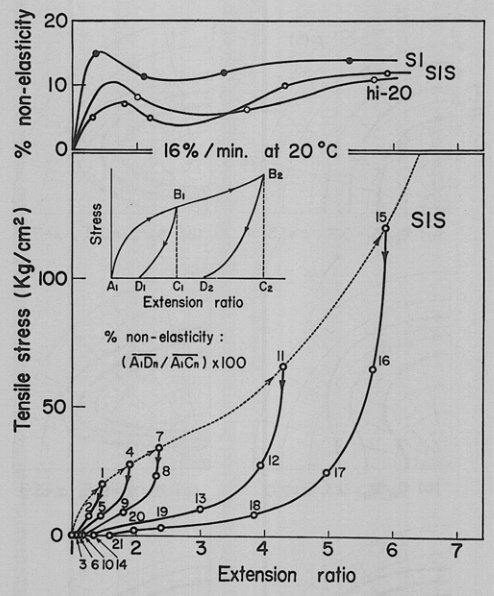

Figure 11. Presentations of elastic and nonelastic properties of the specimens; the lower half shows cyclic tensile stress–strain relations of the film specimen of SIS and the upper half illustrates the per cent nonelasticity, as defined in the figure by (A_1D_n/A_1C_n), for the film specimens SIS, SI, and hi-20, as functions of the extension ratios.

some occurrence of permanent entanglement of the middle isoprene blocks with each other, as suggested by swelling experiments,[9,24] and also of anchoring of the ends of the middle isoprene blocks to two different spheres of the styrene component. The restriction of segment mobility of the isoprene blocks must be reflected not only in the stiff and very elastic mechanical properties (which even exceed the reinforcing effect in the case of hsS-20, as illustrated in Figure 2) but also in the marked change of the V_v pattern with stretching.

Elastic Recovery. Figure 11 represents some elastic and nonelastic properties of the specimens, *i.e.*, the lower half of the figure shows cyclic tensile stress–strain relations of a particular specimen, SIS, while the upper half of the figure illustrates the per cent nonelasticity of the specimens SIS, SI, and hi-20, as defined in the figure by $(\overline{A_1D_n}/\overline{A_1C_n})$, as functions of the extension ratios. As seen in the figure, every specimen shows, in general, considerable elasticity, becoming a little less elastic with increasing extension ratio, except for a peak in the per cent nonelasticity at relatively small extension ratios.

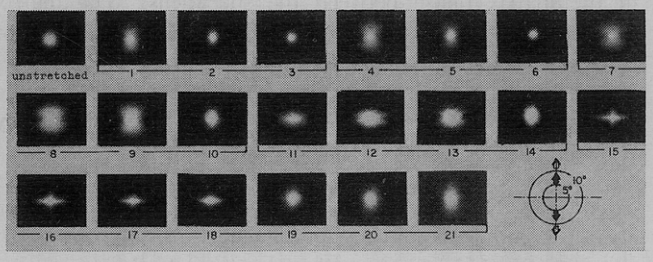

Figure 12. V_v light scattering patterns from film specimens of SIS during recovery of tensile strain from various stretched states. The numbers attached to respective patterns correspond to those along the recovery cycles of tensile strain in Figure 11.

(24) E. T. Bishop and S. Davison, *J. Polym. Sci., Part C*, **No. 26**, 39 (1969).

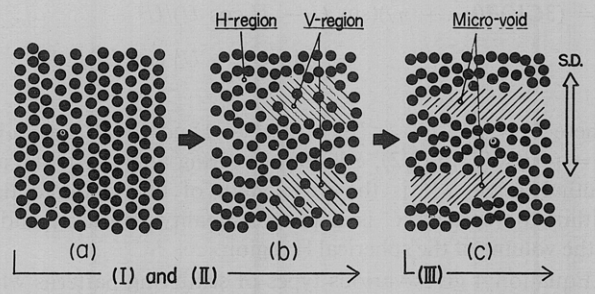

Figure 13. Schematic diagrams proposing a deformation mechanism of elastomeric block copolymers associated with the formation of localized heterogeneous regions of lower density, *i.e.*, V regions: (a) para crystalline arrangement of the spherical domains in unstretched state, (b) formation of V and H regions (in H regions the interdomain distance along the stretching direction is slightly larger than that in the unstretched state), (c) growth of microvoids at the ultimate state of the V region.

Figure 12 shows the change in the V_v light scattering pattern during the recovery cycles of the stress–strain relations of the SIS specimen from various extension ratios, where the numbers attached to the respective patterns correspond to those along the recovery cycles of the stress–strain curves in Figure 11. As easily recognized from the figure, the V_v scattering patterns revert to the original circular pattern of type A in Figure 8 unless the cyclic deformations are exceeded beyond region I. On the other hand, when cyclic deformations are performed beyond region I, especially when ranging into region III, the V_v pattern observed after the elastic recovery is no longer the circular pattern of type A but the ellipsoidal pattern of type B, having its semimajor axis parallel to the stretching direction, as seen in numbers 10, 14, and 21 in the figure. This suggests that a part of the V region is left unrecoverable, thereby creating the source of nonelasticity in these materials.

Conclusions

The deformation mechanism of elastomeric block copolymers having spherical domains of a plastic component dispersed in a matrix of rubber component was investigated by means of simultaneous measurements of tensile stress–strain relations, small-angle light scattering, and small-angle X-ray scattering.

The deformation of these materials is highly elastic over a wide range of extension ratios. At small extension ratios, the deformation is associated with a uniform distribution of internal strain throughout the rubber matrix between the spherical domains; but at relatively higher extension ratios, the deformation is accompanied by formation of a heterogeneous region of lower density over a considerable region (a few microns) which is much larger in size than the domain structures formed by the microphase separation of the block segments. This localized heterogeneous region of lower density shows, however, considerable recoverability. The observed nonelasticity may be ascribed to the transformation of the lower density regions into microvoids at the ultimate stage. Morphological changes accompanying the formation of the heterogeneous region of lower density are illustrated schematically in Figure 13.

The elastomeric properties of these materials must be greatly affected by the fracture process in the localized heterogeneous region of lower density, depending on the nature of the rubber chains in the matrix phase, *i.e.*, depending

on whether each rubber chain is anchored to the spherical domain(s) at no chain end, one chain end, or both chain ends and whether each rubber chain has enough mobility to flow into the lower density region to average out the density fluctuations.

Acknowledgments. The authors are deeply indebted to Dr. Y. Itoh and Messrs. K. Yoshimura and M. Nishimura, Pioneering Research and Development Laboratories, Toray Industries, Inc., for kindly arranging for preparation of the electron micrographs, and to Professor H. Tashiro, Institute for Chemical Research, Kyoto University, for kindly arranging for measurements of small-angle X-ray scattering. A part of this work was supported by a grant from the Scientific Research Funds (Kagaku Kenkyu-hi, 85181-1970) of the Ministry of Education, Japan, and grants from the Japan Synthetic Rubber Co. Ltd., Tokyo, Japan, and Bridge Stone Tire and Rubber Co. Ltd., Tokyo, Japan.

Distribution of Long and Short Branches in Low-Density Polyethylenes

E. P. Otocka,* R. J. Roe, M. Y. Hellman, and P. M. Muglia

Bell Telephone Laboratories, Incorporated, Murray Hill, New Jersey 07074.
Received March 2, 1971

ABSTRACT: The distribution of long and short branches in three commercial low-density polyethylenes has been determined by combining gel permeation chromatography, viscometry, and infrared spectra analyses. The results indicate that different manufacturing polymerization conditions can lead to significant departures from ideal branch distribution.

Low-density polyethylene (LDPE) produced in high-pressure reactors is one of the oldest and most important commercial polymers. Its physical properties depend upon the concentration and distribution of both long and short chain branches (LCB and SCB).[1-3] Exact definitions of the structure–property correlations in this regard have not been possible to date. Theroetical and (especially) experimental techniques simply have not been available which permit accurate measurement of LCB, SCB, and their relationship to MWD. The advent of gel permeation chromatography and particularly its universal calibration has afforded the potential of improved analysis.[4-7] The purpose of our effort is to analyze the distribution of LCB and SCB in three commercial low-density polyethylenes by combining gel permeation chromatography with a variety of other techniques. The results are viewed with particular attention to the limitations of current theory.

In the high-pressure polymerization of ethylene, it is generally accepted that LCB arises from intermolecular chain transfer to polymer while SCB is generated by intramolecular H abstraction *via* a cyclic intermediate. Treatments of polymerization under constant conditions (T, P, [M], [PE]) in general predict that

$$\lambda_{LCB} = b/M \qquad (1)$$

where b = number of LCB per molecule; M = polymer molecular weight; and λ_{LCB}, called the long-chain branching coefficient,[8-10] is a constant independent of extent of reaction or molecular weight. This prediction has been apparently confirmed in some cases.[6,7,11,12] In the variety of commercial high-pressure polymerization reactors employed, however, it seems unlikely that the uniform conditions necessary to validate eq 1 apply. Therefore we doubt the generality of eq 1 and suggest that variations in λ with M can provide useful data for the characterization of LDPE'ss.

The analysis of LCB revolves about the observation that branched chains occupy a smaller volume in solution than linear molecules of the same molecular weight. There are a number of experimental techniques available to measure the dimensions of polymer molecules in solution: intrinsic viscosity, $[\eta]$; translation friction coefficient, Ξ; light scattering, the limit of K_C/R_θ as C approaches zero; and gel permeation chromatography elution volume, V_e. In the cases of Ξ, the dimension derived is the Stokes' radius R_H, and, for the limit of K_C/R_θ as $C \rightarrow$ zero, the radius of gyration, R_G. Interpretation of $[\eta]$ and V_e in terms of molecular size involves a degree of ambiguity, especially for branched polymers. An equivalent hydrodynamic radius, R_e, is defined by $[\eta]$ and may be correlated with V_e.[13] The supposedly simple relationship between R_e and R_G for linear polymers has been the subject of continued study[14,15] and is virtually unknown for branched polymers. Experimental and theroetical studies have indicated a V_e–R_G correlation, but the matter is not resolved.[4,13,16] The basic problem is simply that the mechanism of separation in gel permeation chromatography has not been completely defined

(1) M. L. Miller in "The Structure of Polymers," Reinhold, New York, N. Y., 1966.
(2) M. Morton, T. E. Helminiak, A. D. Gadkary, and F. Beuche, *J. Polym. Sci.*, **57**, 471 (1962).
(3) W. W. Graessley in "Characterization of Macromolecular Structure," D. McIntyre, Ed., National Academy of Sciences, Washington, D. C., 1968.
(4) E. Grubisic, P. Rempp, and H. Benoit, *J. Polym. Sci., Part B*, **5**, 753 (1967).
(5) L. H. Tung, *ibid., Part A-2*, 7, 47 (1969).
(6) R. A. Mendelson and E. E. Drott, *ibid., Part B*, **6**, 795 (1968).
(7) E. E. Drott and R. A. Mendelson, *ibid., Part A-2*, **8**, 1361, 1373 (1970).
(8) J. K. Beasley, *J. Amer. Chem. Soc.*, **75**, 6123 (1953).
(9) W. H. Stockmayer, *J. Chem. Phys.*, **11**, 45 (1943).
(10) O. Saito, K. Nagasubramanian, and W. W. Graessley, *J. Polym. Sci., Part A-2*, **7**, 1937 (1969).
(11) L. Wild and R. Guliana, *ibid., Part A-2*, **5**, 1087 (1967).
(12) A. R. Shultz, *Eur. Polym. J.*, **6**, 69 (1970).
(13) K. A. Boni, F. A. Sliemers, and P. B. Stickney, *J. Polym. Sci., Part A-2*, **6**, 1579 (1968).
(14) O. B. Ptitsyn and Y. E. Eisner, *Zh. Tekh. Fiz.*, **29**, 1117 (1959).
(15) G. C. Berry and T. G. Fox, *J. Amer. Chem. Soc.*, **86**, 3540 (1964).
(16) E. F. Casassa and T. Yagami, *Macromolecules*, **2**, 14 (1969).